Annales
Geophysicae

Open Access

Mesospheric front observations by the OH airglow imager carried out at Ferraz Station on King George Island, Antarctic Peninsula, in 2011

Gabriel Augusto Giongo[1,2], **José Valentin Bageston**[1], **Paulo Prado Batista**[3], **Cristiano Max Wrasse**[3], **Gabriela Dornelles Bittencourt**[2], **Igo Paulino**[4], **Neusa Maria Paes Leme**[5], **David C. Fritts**[6], **Diego Janches**[7], **Wayne Hocking**[8], **and Nelson Jorge Schuch**[1]

[1]Southern Regional Space Research Center, National Institute for Space Research, Santa Maria – RS, 97105-970, Brazil
[2]Federal University of Santa Maria, Santa Maria – RS, 97195-000, Brazil
[3]Aeronomy Division, National Institute for Space Research, São José dos Campos – SP, 12227-010, Brazil
[4]Federal University of Campina Grande, Campina Grande – PB, 58.429-900, Brazil
[5]Northern Regional Center, National Institute for Space Research, Natal – RN, 59076-740, Brazil
[6]Boulder GATS, Inc., Boulder, CO 80301, USA
[7]Space Weather Laboratory – Goddard Space Flight Center, National Aeronautics and Space Administration, Greenbelt, MD 20771, USA
[8]University of Western Ontario, London, Ontario, N6A 3K7, Canada

Correspondence: Gabriel Augusto Giongo (gabrielgiongo@hotmail.com)

Abstract. The main goals of this work are to characterize and investigate the potential wave sources of four mesospheric fronts identified in the hydroxyl near-infrared (OH-NIR) airglow images, obtained with an all-sky airglow imager installed at Comandante Ferraz Antarctic Station (EACF, as per its Portuguese acronym) located on King George Island in the Antarctic Peninsula. We identified and analyzed four mesospheric fronts in 2011 over King George Island. In addition, we investigate the atmospheric background environment between 80 and 100 km altitude and discuss the ducts and propagation conditions for these waves. For that, we used wind data obtained from a meteor radar operated at EACF and temperature data obtained from the TIMED/SABER satellite. The vertical wavenumber squared, m^2, was calculated for each of the four waves. Even though no clearly defined duct (indicated by positive values of m^2 sandwiched between layers above and below with $m^2 < 0$) was found in any of the events, favorable propagation conditions for horizontal propagation of the fronts were found in three cases. In the fourth case, the wave front did not find any duct support and it appeared to dissipate near the zenith, transferring energy and momentum to the medium and, consequently, accelerating the wind in the wave propagation direction (near to south)

above the OH peak (88–92 km). The likely wave sources for these four cases were investigated by using meteorological satellite images and in two cases we could find that strong instabilities were potential sources, i.e., a cyclonic activity and a large convective cloud cell. In the other two cases it was not possible to associate troposphere sources as potential candidates for the generation of such wave fronts observed in the mesosphere and secondary wave sources were attributed to these cases.

1 Introduction

Atmospheric gravity waves have been an expanding research area in the last years due to several effects and contributions of these waves in the atmospheric circulation, structure, and variability (Fritts and Alexander, 2003).

In addition to the vertical transport of momentum and energy, the gravity waves also are important when they are sub-

ject to some process of channeling, which inhibits vertical propagation, trapping the flux of energy and momentum to a limited range of altitudes (Chimonas and Hines, 1986).

Since the discovery of the wave fronts, commonly called mesospheric bores (Taylor et al., 1995), several reports have been published on both experimental research (Li et al., 2013; Narayanan et al., 2012; Walterscheid et al., 2012; Medeiros et al., 2016) and modeling of the phenomenon (Seyler, 2005; Laughman et al., 2009; Fritts et al., 2013; Snively et al., 2013).

Unlike low- and mid-latitudes, where mesospheric fronts are a relatively common wave type and have been identified (by Taylor et al., 1995; Smith et al., 2003; Medeiros et al., 2005, 2016; Fechine et al., 2005; Smith, 2014), just a few cases have been reported for sub-Antarctic latitudes (e.g., Nielsen et al., 2006; Stockwell et al., 2006; Bageston et al., 2011a, b; Dalin et al., 2013). Bageston et al. (2009) in their observations at Ferraz Station, during 2007, observed more than 230 gravity wave events, but only two clear cases of mesospheric fronts were reported. The first one was a mesospheric wall (Bageston et al., 2011a) and the second one was a mesospheric bore (Bageston et al., 2011b). In both cases, the fronts were supported by stable ducts (the first one a thermal duct and the second one a thermal-Doppler duct). Also, from observations over Halley Station, Antarctica (76° S, 27° W), with two consecutive years of data and a large number (221 wave band type) of mesospheric gravity waves (Nielsen et al., 2009), only one case was reported as a bore event (Nielsen et al., 2006). Thus, from these previous reports for the Antarctic Peninsula and low-mid latitudes, one can infer that mesospheric fronts are very uncommon events in the sub-Antarctic islands ($\sim 62°$ S) and near the border of the Antarctic continent (76° S).

In this paper, we present the physical parameters for the four mesospheric fronts identified. We examine the atmospheric conditions of the medium in which these events propagated, using temperature data obtained from the TIMED/SABER instrument and wind data obtained from the meteor radar installed at Ferraz Station. We also discuss the propagation conditions for the four waves and the impact of one wave front in the upper mesosphere, mainly on the mean wind, when it dissipates. Lastly, an analysis of the sources for these mesospheric fronts is performed, using satellite images, in order to associate the tropospheric conditions to the generation of these waves.

2 Instrumentation and methodology

The visualization of the mesospheric fronts was made by using airglow images obtained with an all-sky CCD imager (SBIG, STL-1001E model) installed in a shelter close to the Ferraz Station (~ 1.0 km), but hiding behind a hill in order to avoid the light contamination from the main station. The system uses a near-IR filter with a pass band in the range 715–930 nm, with a notch at 865.5 nm to suppress the O_2 (0–1) emission, to isolate the OH emission with a peak at approximately 87 km altitude (the nominal emission altitude). A telecentric lens is coupled with a high-resolution CCD, 1024×1024 pixels, 24.6×24.6 mm and $\sim 50\%$ of quantum efficiency in the near-infrared. The exposure time of the images was 20 s and due to the limitations of the optical system, which was not originally designed for the camera, the images were cropped to 512×512 pixels (Bageston, 2011a).

In the calibration process, it is possible to generate four linear projections (km $\times$ km) for the unwarped images, that is 256×256, 512×512, 768×768, and 1024×1024. For the current analyses, we used the projection of 512 km $\times$ 512 km, which gives a resolution of 1.0 km pixel^{-1} (512 km per 512 pixels), because the wave fronts appeared clearly in this projection.

In order to obtain the parameters of the observed fronts, a two-dimensional FFT (fast Fourier transform) was used, following the methodology described by Wrasse et al. (2007). The methodology consists of selecting a rectangular area in a sequence of 4–5 images; this area must contain the oscillation on all selected images where the front can be seen clearly, without the Milky Way contamination, and this area must contain the wave structure. The horizontal wavelength, observed phase speed, and observed period are obtained from the Fourier spectra.

The wind data were obtained from the meteor radar installed in EACF. The radar consists of eight transmitting Yagi antennas arranged in a circle of 24.4 m, five receiving antennas arranged in an asymmetric cross, and a receiver module. Its operation is on an emission frequency of 36.9 MHz, bandwidth ranging from 35 to 125 kHz, and a power emission peak of 30 kW (Fritts et al., 2012). The radar emits pulses at the above frequencies that are reflected by the trail of gas left by the meteors as they enter in the atmosphere, and this trail is subjected to the local winds. In this way, by the received signal, the radar can measure the wind components in the meteor region, at about 70–110 km height. The methodology behind the estimation of winds is based on a complex correlation adopted to measure the signal phase differences between the receiving antennas in order to determine the echo arrival angle, and complex auto- and cross-correlation methods are used to obtain the rate of change of the relative phase in order to determine the radial velocity associated with the meteor trail, and then the meteor radar provides hourly zonal and meridional winds (John et al., 2011).

Temperature data obtained from the Sounding of the Atmosphere using Broadband Emission Radiometry (SABER) instrument on board the Thermosphere, Ionosphere, Mesosphere, Energetics and Dynamics (TIMED) satellite (Mertens et al., 2001, 2004) were used to calculate the buoyancy frequency (N^2) and the squared vertical wave number (m^2). The SABER instrument retrieves the temperature in a wide range of altitudes (~ 15–129 km) based on the non-local thermodynamic equilibrium in the mesosphere
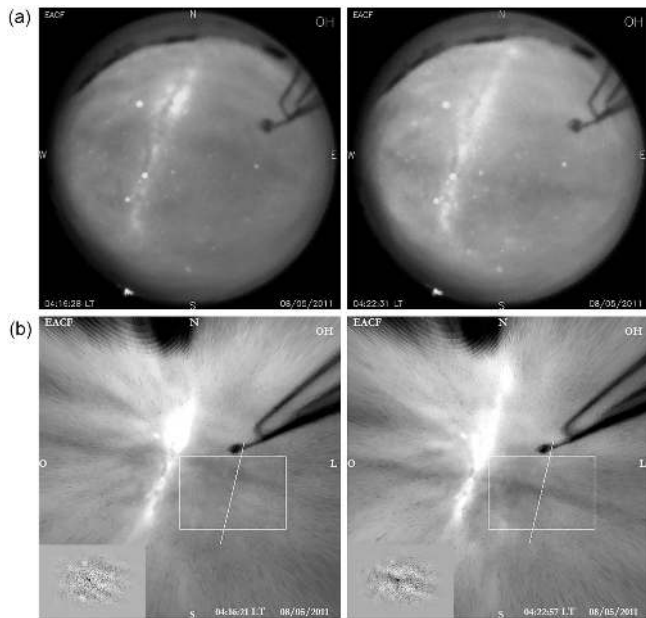
Figure 1. Original airglow images **(a)** and unwarped images **(b)** used for the spectral analysis of the gravity waves. This mesospheric front was observed on 8 May and characterized with images from 07:15 to 07:23 UT. The lower panels show the images with the star field removed and a small region used for analysis (selected white box), already filtered by a high-pass filter.

and lower thermosphere (MLT) region (Mertens et al., 2009). The TIMED/SABER satellite also provides the volume emission rate (VER) of the OH airglow emission between 60 and 100 km height, which is very important in the present study, mainly in the coincident altitudes of the meteor radar measurements.

3 Airglow observations and analysis

Four mesospheric fronts were observed over the Brazilian Antarctic station during the year 2011. The first event occurred on the night of 7–8 May at 07:16 UT, the second wave front on 22–23 August at 03:21 UT, the third event on 27–28 August at 22:35 UT, and the last reported event was observed on 28–29 August at 00:14 UT.

Figure 1 shows two airglow images for the first frontal event observed in 2011. The first row is the set of two original images and the second row shows the same images but unwarped, where we can see the selected region (white box) in the image for the analysis. The line crossing the box indicates the front propagation direction, while in the bottom left corner the small image is a post-processed (filtered) sub-image used in the spectral analysis. By a visual analysis of the images in Fig. 1, it is possible to identify a wall event propagating south. From the Fourier analysis, the obtained parameters for this event were the following: horizontal wave-
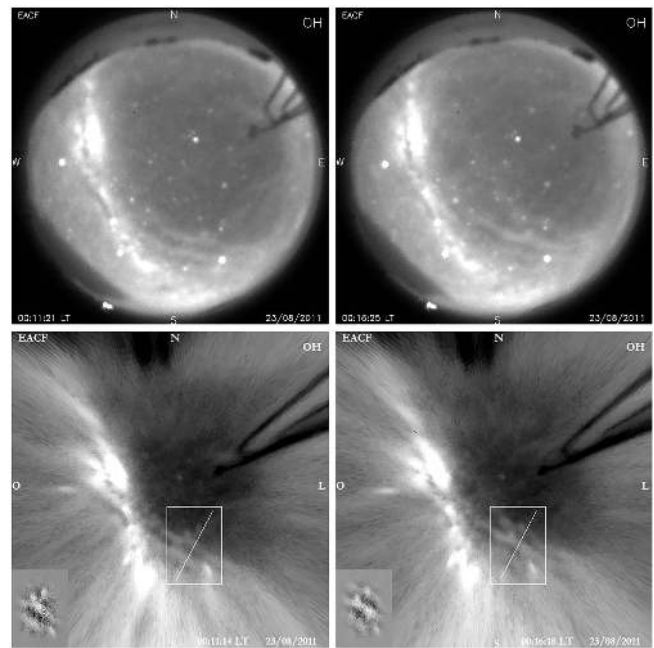

Figure 2. Same as Fig. 1 but for the mesospheric front characterized from 03:11 to 03:16 UT on 23 August.

length of 33.8 ± 3.0 km, observed period of 6.0 ± 0.6 min, observed phase speed of 75.9 ± 5.8 m s^{-1}, and an azimuthal propagation direction of $193.2 \pm 5.1°$ (southwest). This event appeared in the images at 07:16 UT and about 15 min later it was followed by a large wave structure, in a similar way to recent results presented by Smith et al. (2017); However, in our case it was not possible to associate the possible front generation to this large disturbance structure since we have a weak medium-scale disturbance that occurred nearly orthogonal to the mesospheric front and appeared in the images when the front was already near the zenith.

The second event was a front followed by a wave train and an increase in its brightness, and the wave event lasted in the field of view of the all-sky imager for at least 1 hour. However, from 03:30 UT another gravity wave (band type) from the east disturbed the wave train of the mesospheric front, which dissipated during the interaction between the two waves. Figure 2 presents the observation of the second mesospheric front, during the time in which their parameters were analyzed. The first row shows the original airglow images and the second row shows the post-processed images for the spectral analysis. In this case, the obtained parameters, considering the wave train, were the following: wavelength of 23.7 ± 2.6 km, period of 4.7 ± 0.4 min, phase speed of 84.7 ± 5.5 m s^{-1}, and propagation direction of $33.7 \pm 1.7°$ (northeast). Considering only the wave front, it was observed with a phase speed of 89 ± 9.7 m s^{-1} with a propagation direction nearly to the north.

The third reported event was observed as a dark front followed by a small wave train (not very well defined). Figure 3
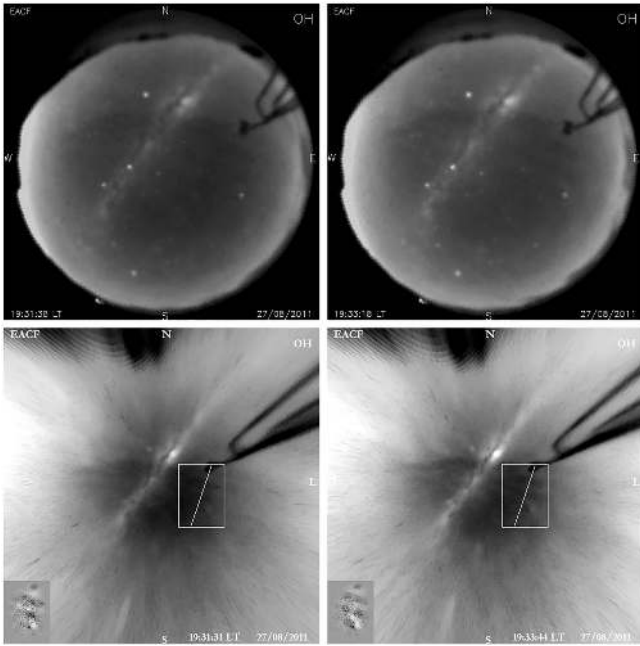
Figure 3. Same as Fig. 1 but for the mesospheric front characterized from 22:30 to 22:34 UT on 27 August.

Figure 4. Same as Fig. 1 but for the mesospheric front characterized from 00:14 to 00:25 UT 29 August.

shows the observed event in the original images (first row) and it is possible to see the front propagating to the north, followed by small ripples which we can infer to be the wave train. In the second row of Fig. 3, we see the ripples with the box used in order to obtain the wave parameters. The parameters observed for this small wave train were the following: wavelength of 23.1 ± 2.2 km, period of 12.6 ± 1.4 min, phase speed of 30.6 ± 2.9 m s^{-1}, and a propagation direction of $18.4 \pm 5.0°$ (north). For the main front, it was observed with a phase speed of 43.9 ± 4.6 m s^{-1} and a propagation direction of $356 \pm 4.7°$ (north). The large difference in the propagation direction was due to the location in which the box was placed for the analysis of the front and the wave train. The velocity obtained for this event is quite uncommon, i.e., very low as compared to other typical fronts. This is likely due to the action of the wind decelerating the wave. This will be discussed again in the next section.

Figure 4 shows the last observed event, where the first row shows the original images and the second row presents the respective unwarped images. The analysis for this case resulted in a wavelength of 22.1 ± 2.0 km, period of 5.4 ± 0.4 min, phase speed of 68.4 ± 4.5 m s^{-1}, and a propagation direction of $187.4 \pm 3.0°$ (south). The front presented a phase speed of 52.2 ± 5.2 m s^{-1} and a propagation direction of $187.6 \pm 3.5°$ (south). All of the parameters for this case and the previous ones are reported as observed parameters. Table 1 summarizes the observed parameter results for the mesospheric fronts described above, together with the fronts identification and date of occurrence.
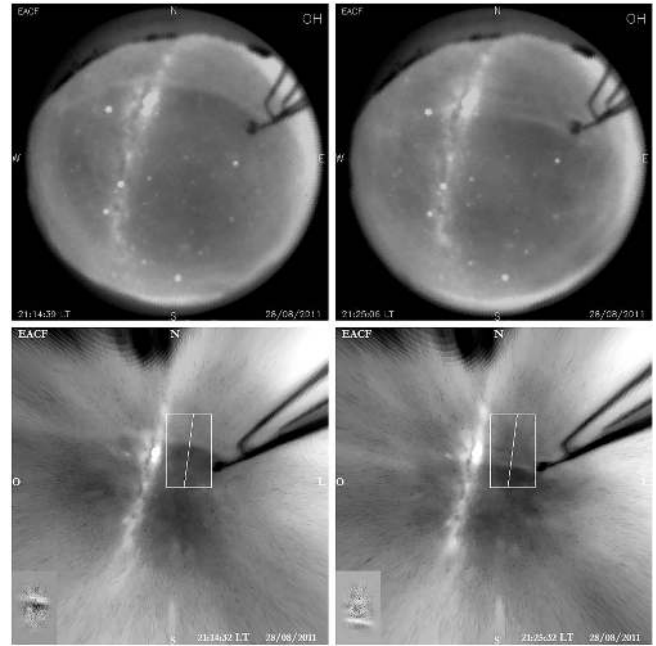
We should emphasize that all of the mesospheric fronts showed a step function like the leading fronts. In two cases, the fronts as a minimum of airglow emission (dark fronts) and the other two presented a maximum brightness in the airglow emission. Among the four analyzed cases, only one showed a remarkable wave train, while two of them were basically single fronts (wall-type front) followed by small ripples, and another one appeared as a wide dark region (not too extensive) propagating into a bright region.

4 Atmospheric environment and propagation conditions

In order to characterize the atmospheric duct where these mesospheric fronts propagated, we analyze the vertical propagation condition of each front using the Taylor–Goldstein equation:

$$m^2 = \frac{N^2}{(u-c)^2} - \frac{u''}{u-c} - k_h^2. \tag{1}$$

In Eq. (1), m^2 is the vertical wavenumber, u is the wind speed in the wave direction, u'' is the second derivative term of the wind speed, c is the observed wave phase speed, k_h is the horizontal wavenumber, and N is the buoyancy frequency, given by the following equation.

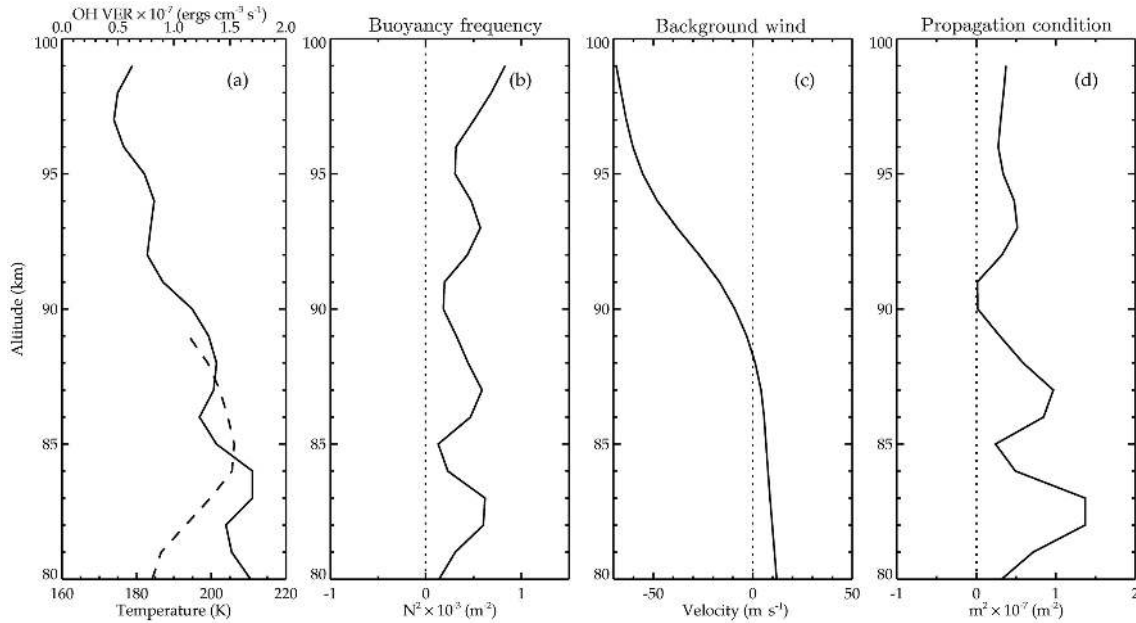$$N^2 = \frac{g}{T}(\nabla T_Z + \frac{g}{C_P}) \tag{2}$$

Figure 5. Atmospheric profiles for **(a)** temperature (solid line) and OH volume emission rate (OH-VER, dashed line), **(b)** buoyancy frequency (N^2), **(c)** wind profile in the wave propagation direction and **(d)** vertical propagation condition (m^2). In this case the profiles were obtained for the mesospheric front observed on 5 May 2011.

Table 1. Mesospheric fronts observed in 2011 at Ferraz Station and their respective parameters.

Event	Date and time (UT)	Horizontal wavelength (km)	Period (min)	Azimuthal direction (°)	Phase speed (m s^{-1})
1	08 May, 07:16	$33.8 \pm .30$	6.0 ± 0.6	187.6 ± 5.1, S	75.9 ± 5.8
2	23 Aug, 03:11	23.7 ± 2.6	4.7 ± 0.4	33.7 ± 1.7, NE	89.0 ± 9.7
3	27 Aug, 22:32	23.1 ± 2.2	12.6 ± 1.4	18.4 ± 5.0, N	43.9 ± 4.6
4	29 Aug, 00:10	22.1 ± 2.0	5.4 ± 0.4	187.4 ± 3.0, S	52.8 ± 5.2

In the above equation, g is the acceleration due to gravity, T is the temperature, C_P is the specific heat at constant pressure, and ∇T_Z is the temperature gradient.

Equation (1) is a dispersion relation valid for gravity waves propagating in an environment where the effects of horizontal winds and temperature gradients cannot be neglected (Chimonas and Hines, 1986; Isler et al., 1997; Fritts and Yuan, 1989). The analysis of this equation can provide the wave propagation conditions; that is, if $m^2 > 0$, then the wave can freely propagate vertically; if $m^2 < 0$, then the wave is not allowed to propagate vertically; and, lastly, in the case where the region of $m^2 > 0$ is surrounded by two regions of $m^2 < 0$, this interval of $m^2 > 0$ is called a ducted region.

Then, based on the Eqs. (1) and (2) and using temperature data from the SABER instrument, and wind data from the meteor radar, one can estimate if the required ducts for the events to propagate exist. In the case of confirmation of favorable conditions for ducted waves, then it is possible to analyze if the duct was due to the temperature structure (ther-

mal duct), basic wind contribution (Doppler duct), or contributions from both temperature and wind (thermal-Doppler duct).

Figure 5 shows the vertical profiles for the atmospheric environment and propagation conditions for the first event, which occurred between 7–8 May. Figure 5a shows the vertical temperature profile (solid line) with the OH volume emission rate (OH-VER; dashed line), using the closest SABER sounding to the EACF, Fig. 5b shows the buoyancy frequency calculated with the temperature shown in Fig. 5a. Figure 5c presents the wind profile in the direction of wave propagation, and finally, Fig. 5d shows the m^2 propagation condition. For the night of 7–8 May there were just a few SABER soundings near the EACF and the closest sounding was about 4 h before the event occurrence and distant ~ 300 km from the station. The temperature profile presented in Fig. 5a is an approximation of the thermal environment in the surroundings of the station from where the front was identified, because it is very difficult to obtain simultaneous SABER
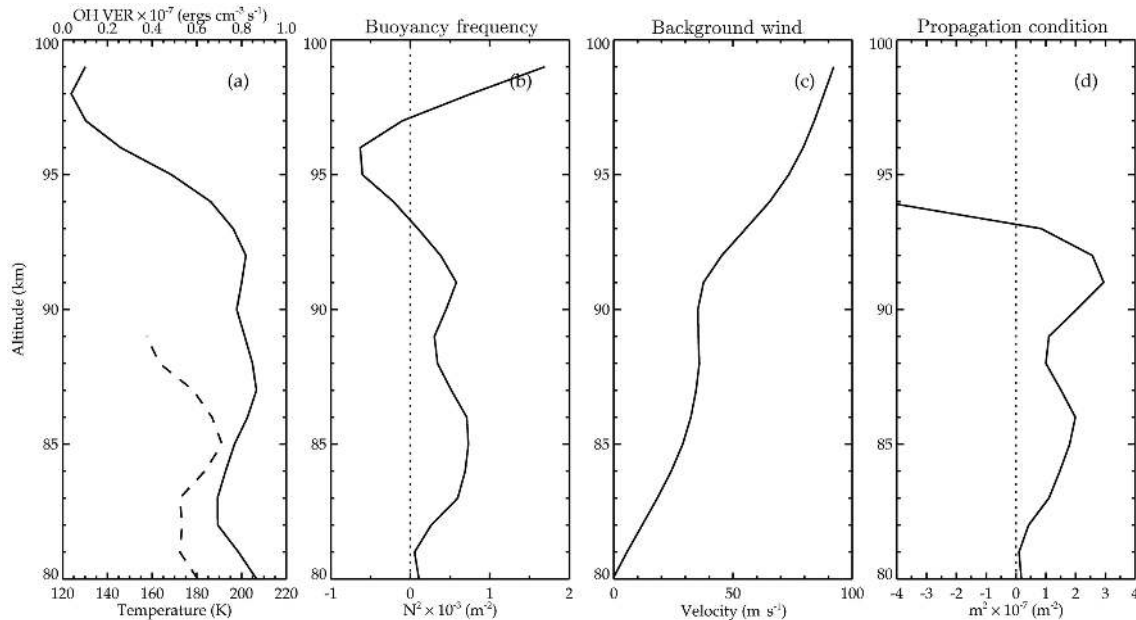
Figure 6. Same as Fig. 5 but for the mesospheric front observed on 23 August 2011.

observations with a rare gravity wave event, especially for Antarctic latitudes. From the OH-VER emission observed by the TIMED/SABER satellite, it is possible to identify the peak height of the OH airglow emission. As can be seen in Fig. 5, the front was confined between about 82 and 90 km height where $m^2 > 0$, with the emission peak around 85 km height and a double duct structure in this altitude interval, but with the main duct associated with this wave front between 80 and 85 km. None of the graphs were plotted below 80 km because there was no wind measurements below this height. In this case, we can infer that the approximate duct formation is characterized mainly by the temperature vertical structure (thermal favorable condition), since the m^2 profile is very similar to the buoyancy frequency and the wind profile did not show significant variation ($\sim 10.0\,\mathrm{m\,s^{-1}}$) from 80 to 89 km height. However, this condition (not a true duct) could maintain the wave front to be quite stable and propagating mainly horizontal, but also vertically ($m^2 > 0$).

Figure 6 shows the vertical profiles for the atmospheric environment and propagation conditions for the second event, which occurred between 22–23 August. The graphs in Fig. 6 represent the same variables and in the same way as presented in Fig. 5, but now for the parameters of the second wave front. For this day, the closest SABER sounding was obtained approximately 5 h before the observed time of this event and 420 km away from EACF. In Fig. 6a, it is observed that the OH emission layer is located between 81 and 88 km, with the peak at 85 km, so we focus the analysis in this altitude interval, even though the more pronounced m^2 is located above 90 km height. The temperature is decreasing from 80 to 82 km and then turns to increasing up to 87 km, and this

small inversion leads to duct-like in the buoyancy frequency and also in the m^2 profile in this altitude interval. Again, the propagation condition is similar to the previous case, having no influence by wind conditions in the region of the OH airglow layer. Thus, the duct-like condition for this case was also caused by the temperature.

Figure 7 shows the atmospheric background environment and propagation conditions for the third event. In this case, we can see a clear correlation between the background wind and m^2. A duct is clearly visible centered on 86 km, several km above the OH peak which is located at 81 km. It is noteworthy that the m^2 is very near to an ideal duct condition, although m^2 does not become negative below 82 km and above 92 km, because the temperature profile did not contribute to the formation of this ideal duct. It is also noted that two strong inversions in the wind occur at 82 and 91 km height and this wind shear generated the ideal conditions for a Doppler duct. Another interesting aspect for this case is the fact that the wave has a phase speed approximately equal to the wind speed; consequently, the two wind shears that characterize the duct were absorbing the wave energy as the wave was approaching the critical level (Nappo, 2002). The closest temperature profile used was obtained about to 2.5 h before the wave front occurrence and approximately 370 km away from Ferraz Station (inside the field-of-view of the all-sky imager), but this temperature did not influence the formation of the duct.

The environment and propagation conditions for the last event are shown in Fig. 8, in the same format as in the previous figures. The SABER profiles were obtained about 4 h before the occurrence of this wave front, i.e., it is a rough ap-
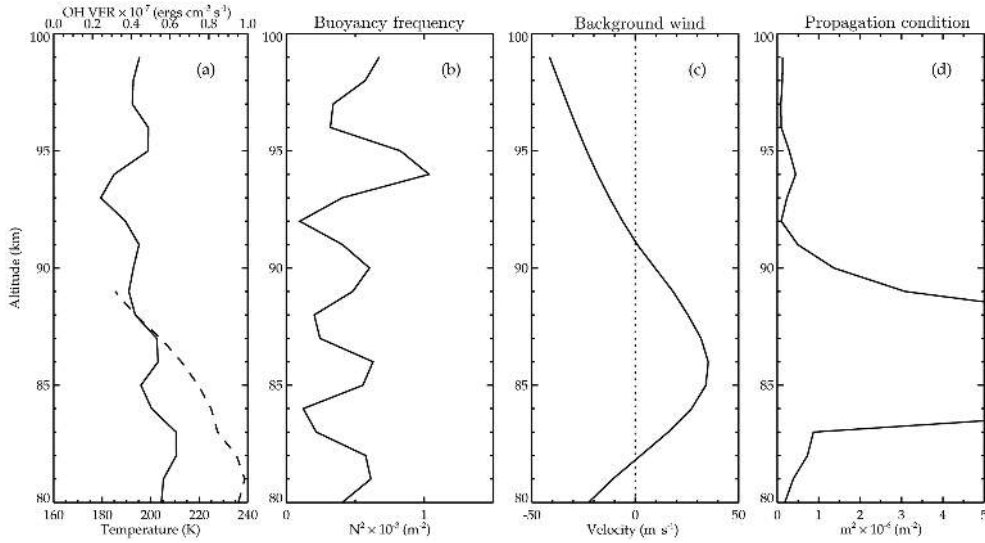
Figure 7. Same as Fig. 5 but for the mesospheric front observed on 27 August 2011.
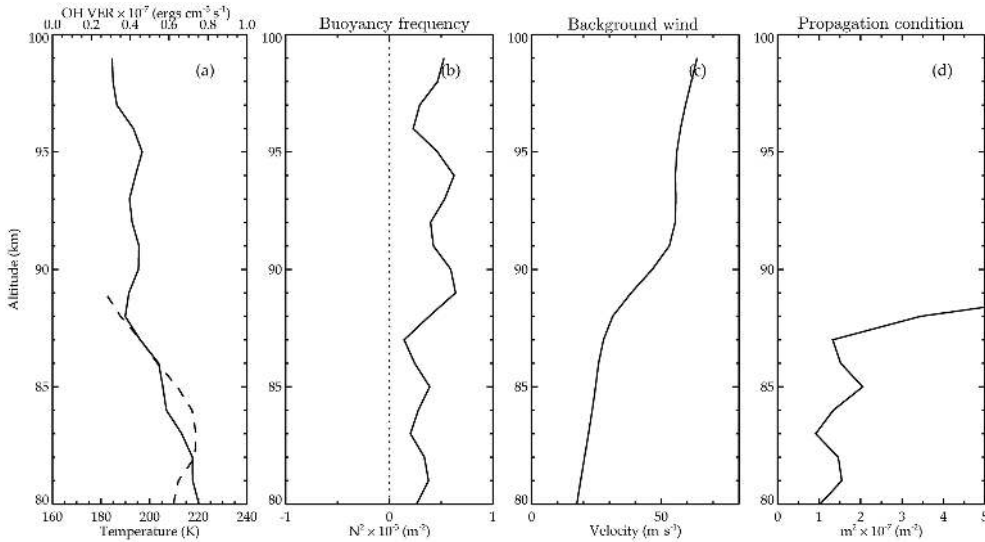

Figure 8. Same as Fig. 5 but for the mesospheric front observed on 29 August 2011.

proximation for the temperature at the instant of occurrence of the front and may not represent the thermal structure over the observatory around the time of the wave front observation. The temperature profile within the OH layer presented a small and constant decreasing rate ($\sim 3\,\mathrm{K\,km^{-1}}$), between 81 and 86 km, without significant variability, so did not form a thermal duct configuration, as observed in the N^2 profile in Fig. 8b. On the other hand, the wind profile along the wave direction (obtained between 00:00 and 01:00 UT), as shown in Fig. 8c, was relatively weak and almost constant between 80 and 88 km height. The wind characteristics coupled with the thermal conditions were not enough to generate a duct configuration, as can be noted in Fig. 8d. In this way, the m^2 did not present a duct, i.e., the front could be considered to

be vertically propagating considering the above observed atmospheric background even knowing that this kind of wave needs a duct structure, which was not observed due to the lack of satellite data close to the time of the wave observation. These conditions coupled to other gravity waves propagating simultaneously, and almost orthogonal, caused a destruction of this wave front around 00:43 UT (see the respective video in the Supplement), just after passing the zenith. We suggest that in this case, the wave structure was absorbed by the local environment and contributed to accelerate the background wind, as observed between 90 and 95 km height in Fig. 8c and also in the Supplement (last slide of the .pdf file), where it is noted at 01:30 UT around 93 km height.
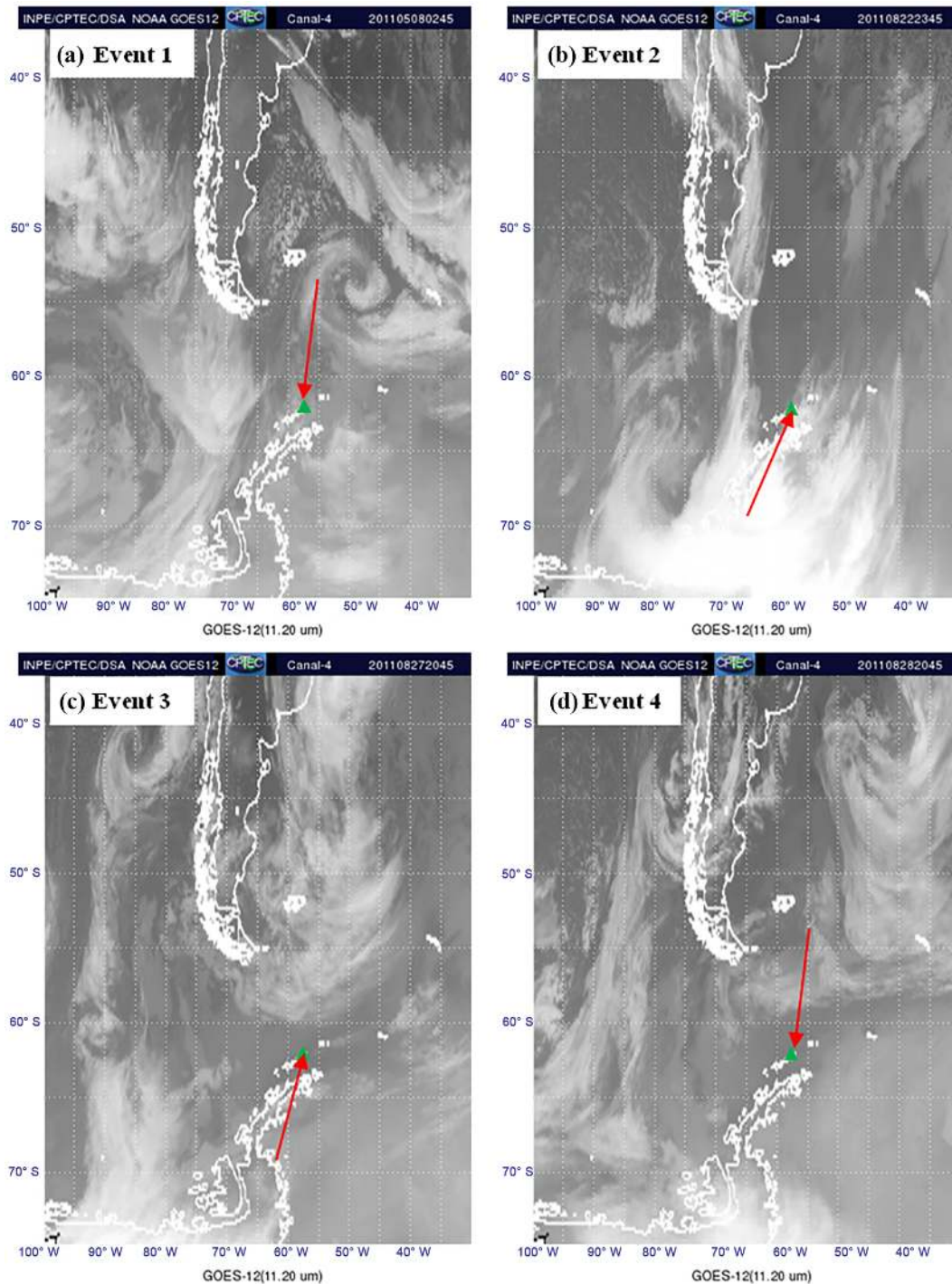
Figure 9. Satellite images before the mesospheric observations. The green triangle represents the position of Ferraz Station and the arrows represent the direction of the front propagation. Event 1 occured approximately 5 hours before the observation of the front, Event 2 about 3 hours before the observation, Event 3 about 2 hours before the observation, and Event 4 about 4 hours before the observation. Source: Center for Weather Forecasting and Climate Studies of the National Institute for Space Research (CPTEC/INPE).

5 Discussion

At first, it is interesting to note that we have observed four wave front events in the whole year of 2011 but three were observed in a single week at the end of August, which means that some anomalous phenomena would be occurring in the surroundings of the Brazilian Antarctic station (directly in

the troposphere or indirectly in the mesosphere). Thus, to investigate the origin of such mesospheric fronts, we analyzed satellite images to look for instabilities or forcing structures, which could generate theses waves. Figure 9 shows four satellite images a few hours before the events observed in the mesosphere. Additionally, an animation (.gif file) for each observed day was added as a Supplement.

The first event is similar to a peculiar wave event reported by Smith et al (2017) who presented a twin bore event that occurred over Europe in March 2013 and their analysis suggested that these bores were associated with a larger-scale mesospheric disturbance, which was associated with a severe meteorological phenomenon (cold front). In our observation, the similarity is based on the fact that we also observed a large-scale disturbance after the front has passed the zenith, just behind the mesospheric front. However, in our observation, the mesospheric disturbance was tenuous and difficult to identify, and was possibly not the proper source of this mesospheric front. On the other hand, 5 h before the front observation, a cyclonic system was present north of Ferraz Station, as can be seen in Fig. 9a. This kind of system is a potential wave source already identified and linked to gravity waves in the mesosphere near the Antarctic Peninsula (Bageston et al., 2018). The cyclones are commonly observed around the peninsula and have been reported by several authors (e.g., Heinemann, 1990; Carrasco et al., 2003). Cyclones can release a large amount of energy into the atmosphere due to the fact that rotational kinetic energy is converted to linear kinetic energy, which in turn generates hydrodynamic instability. This kind of instability is able to generate gravity waves that can propagate up to the mesosphere. Thus, in this first case, we are associating the frontal wave observed in the OH airglow layer to a cyclonic activity in the troposphere, which match very well with the typical time of propagation of the gravity waves from the troposphere to the mesosphere (2 to 6 h) and also because the location of the meteorological system is exactly at the location from where the wave in the mesosphere was observed to come from.

The second mesospheric wave front event is quite similar to the event described by Bageston et al. (2011b) in terms of its morphology, i.e., a remarkable wave front followed by a series of wave crests confined in a very well-defined duct, with the main contribution from the wind structure, but different from the present case, which showed a thermal duct condition for the front propagation. For this case, the potential source in the troposphere is shown in Fig. 9b which presents a large cloud condensate south of Ferraz Station, with a large potential of convective instability as can be seen in the animation (.gif) posted as Supplement, because the clouds near the center of the condensate are very high and much colder ($< -70\,°C$) than the surroundings (-30 to $-50\,°C$) and in the center of this cloud the convection should be very intense. In this case, the potential source in the troposphere was associated with a strong convection generated from the cloud cell identified in Fig. 9b, and a thermal prop-

agation condition (see Fig. 6b and d) in the mesosphere that allowed the wave to propagate from the Antarctic Peninsula to the observatory (Ferraz Station).

For the third event, Fig. 9c shows no evidence of any meteorological phenomena able to generate gravity waves in the troposphere. Also, the dark wave front (a wide depletion airglow region) seen in the all-sky images was not very well defined and we can infer that this observed wave in the mesosphere was generated by a wave–wave interaction or from wave breaking at lower mesospheric heights. As this front was vanishing, it is very likely that such a front was absorbed by the background once the wind was increasing fast in the same direction of the wave propagation (inside the OH layer), as noted in Fig. 7c between 81 and 85 km height, and at some point the wave speed reached the same velocity as the wind. So, for this wave front, the associated source was linked to a dynamical disturbance at mesospheric heights and its dissipation occurred by the wind blowing in the same direction as the wave propagation direction.

The fourth front event was very similar to the third one, but they were propagating in opposite directions. Analogously to the previous case we check the tropospheric situation during the night of the observed event, this is presented in Fig. 9d and it can be noted that no meteorological phenomenon is seen in a radius 1000 km north of the station. Due to the lack of meteorological conditions to support the generation of this event, we can not associate any tropospheric source as a reliable physical mechanism capable of generating the observed wave front. This indicates that other stratospheric or mesospheric phenomena (such as wave breaking or wind shear) should be claimed as the potential wave source, but it is difficult to access such sources since the only available wind data for the troposphere and stratosphere are the meteorological reanalysis.

The occurrence of mesospheric fronts in the Antarctic Peninsula is quite unusual for that geographical region according to previous works (Nielsen et al., 2006; Bageston et al., 2011a, b). However, the present work reports unusual occurrences of mesospheric fronts above Ferraz Station in 2011, and mainly concentrated in a short period of time (1 week). For these three last cases, only one could be associated with meteorological phenomenon and the other two have possible in situ generation. So, the important contribution of this work is not only the report of four mesospheric fronts but also the idea that the main mechanism responsible for wave front generation may not be in the troposphere.

6 Conclusions

In this work, we presented four cases of mesospheric fronts observed at the Brazilian Antarctic station in 2011, by using combined all-sky airglow images with data from a co-located meteor radar and the TIMED/SABER satellite. Three of the four reported cases were observed in a single week at the end

of August and the other case was observed in May. The wave front propagation directions were very distinct from one another, with one wave propagating from southwest to northeast, two cases with waves propagating approximately from north to south (one case in May and the other in August), and in the other case the wave was seen to propagate nearly from south to north. The wave parameters are shown to be slightly distinct for the observed period, while the horizontal phase speed was quite similar, except for the third case that presented a much smaller wave speed (only about $34\,\mathrm{m\,s^{-1}}$) explained by its dissipation due to the background wind. The main findings in the present paper are the following: (1) in the four case studies, the required ducts for the front propagation did not show to be well-defined, where none presented negative m^2 below or above the duct peak; (2) the favorable propagation condition (positive "duct") for the majority of the cases (three) was defined by the temperature profile (buoyancy frequency), and only one case supported by the background wind; (3) regarding the potential wave sources for the four cases (3a) two cases had their sources associated with tropospheric instabilities; that is, for the wave observed in May it was associated with a cyclonic activity as the main source, and for the other event (23 August) an intense convective system (large cloud condensate) occurred to the south of Ferraz Station. (3b) Two wave fronts could not be linked to any meteorological system and local (mesosphere) wave generation from wave breaking or wave–wave interactions are suggested as potential wave sources for these; one of these fronts was absorbed by the local medium. This work shows that not all of the mesospheric waves (in this case, mesospheric fronts) can be linked directly to meteorological phenomena and even if a model was used to describe the wave paths (i.e., ray tracing), it would be very difficult to find the potential wave sources for the last two cases analyzed here.

Data availability. Contact David Fritts (dave@gats-inc.com) for meteor radar measurements over EACF. SABER measurements are available online in the Internet. Airglow images from EACF can be solicited directly by e-mail to José Valentin Bageston (bageston@gmail.com). The CPTEC/INPE satellite images are available online at: http://satelite.cptec.inpe.br/acervo/goes16.formulario.logic (CPTEC/INPE, 2017).

Supplement. The supplement related to this article is available online at: https://doi.org/10.5194/angeo-36-253-2018-supplement.

Competing interests. The authors declare that they have no conflict of interest.

Special issue statement. This article is part of the special issue "Space weather connections to near-Earth space and the atmosphere". It is a result of the 6° Simpósio Brasileiro de Geofísica

Espacial e Aeronomia (SBGEA), Jataí, Brazil, 26–30 September 2016.

References

Bageston, J. V., Wrasse, C. M., Gobbi, D., Takahashi, H., and Souza, P. B.: Observation of mesospheric gravity waves at Comandante Ferraz Antarctica Station (62° S), Ann. Geophys., 27, 2593–2598, https://doi.org/10.5194/angeo-27-2593-2009, 2009.

Bageston, J. V., Wrasse, C. M., Hibbins, R. E., Batista, P. P., Gobbi, D., Takahashi, H., Andrioli, V. F., Fechine, J., and Denardini, C. M.: Case study of a mesospheric wall event over Ferraz station, Antarctica (62° S), Ann. Geophys., 29, 209–219, https://doi.org/10.5194/angeo-29-209-2011, 2011a.

Bageston, J. V., Wrasse, C. M., Batista, P. P., Hibbins, R. E., Fritts, D. C., Gobbi, D., and Andrioli, V. F.: Observation of a mesospheric front in a thermal-doppler duct over King George Island, Antarctica, Atmos. Chem. Phys., 11, 12137–12147, https://doi.org/10.5194/acp-11-12137-2011, 2011b.

Bageston, J. V., Wrasse, C. M., Andrioli, V. F., Peres, L. V., Gobbi, D., Batista, P. P., Petry, A., Klipp, T. S., and Hibbins, R. E.: Small Scale Gravity Wave Sources near Ferraz Station, King George Island, Antarctica, J. Geophys. Res., in review, 2018.

Carrasco, J. F., Bromwich, D. H., and Monaghan, A. J.: Distribution and Characteristics of Mesoscale Cyclones in the Antarctic: Ross Sea Eastward to the Weddell Sea, Mon. Weather Rev. 131, 289–301, https://doi.org/10.1175/1520-0493(2003)131<0289:DACOMC>2.0.CO;2, 2003.

Chimonas, G. and Hines, C. O.: Doppler Ducting of Atmospheric Gravity-Waves, J. Geophys. Res., 91, 1219–1230, 1986.

CPTEC/INPE: Satellite images Database, available at: http://satelite.cptec.inpe.br/acervo/goes.formulario.logic, last access: 21 December 2017.

Dalin, P., Connors, M., Schofield, I., Dubietis, A., Pertsev, N., Perminov, V., Zalcik, M., Zadorozhny, A., McEwan, T., McEachran,

I., Grønne, J., Hansen, O., Andersen, H., Frandsen, S., Melnikov, D., Romejko, V., and Grigoryeva, I.: First common volume ground-based and space measurements of the mesospheric front in noctilucent clouds, Geophys. Res. Lett., 40, 6399–6404, https://doi.org/10.1002/2013GL058553, 2013

Fechine, J., Medeiros, A. F., Buriti, R. A., Takahashi, H., and Gobbi, D.: Mesospheric bore events in the equatorial middle atmosphere, J. Atmos. Sol-Terr. Phys., 67, 1774–1778, https://doi.org/10.1016/j.jastp.2005.04.006, 2005.

Fritts, D. C. and Alexander, M. J.: Gravity wave dynamics and effects in the middle atmosphere, Rev. Geophys., 41, 1–46, https://doi.org/10.1029/2001RG000106, 2003.

Fritts, D. C. and Yuan, L.: An Analysis of Gravity Wave Ducting in the Atmosphere: Eckart's Resonances in Thermal and Doppler Ducts, J. Geophys. Res., 94, 18455–18466, https://doi.org/10.1029/JD094iD15p18455, 1989.

Fritts, D. C., Janches, D., Iimura, H., Hocking, W. K., Bageston, J. V., and Leme, N. M. P.: Drake Antarctic Agile Meteor Radar first results: Configuration and comparison of mean and tidal wind and gravity wave momentum flux measurements with Southern Argentina Agile Meteor Radar, J. Geophys. Res., 117, D02105, https://doi.org/10.1029/2011JD016651, 2012.

Fritts, D. C., Wang, L., and Werne, J.: Gravity wave-fine structure interactions, Part 1: Influences of fine-structure form and orientation on flow evolution and instability, J. Atmos. Sci., 70, 3710–3734, 2013.

Heinemann, G.: Mesoscale vortices in the Weddell Sea region (Antarctica), Mon. Weather Rev., 118, 779–793, https://doi.org/10.1175/1520-0493(1990)118<0779:MVITWS>2.0.CO;2, 1990.

Isler, J. R., Taylor, M. J., and Fritts, D. C.: Observational Evidence of Wave Ducting and Evanescence in the Mesosphere, J. Geophys. Res., 102, 26301–26313, 1997.

John, S. R., Karanam Kishore Kumar, Subrahmanyam, K. V., Manju, G., and Wu, Q.: Meteor radar measurements of MLT winds near the equatorial electro jet region over Thumba (8.5° N, 77° E): comparison with TIDI observations, Ann. Geophys., 29, 1209–1214, https://doi.org/10.5194/angeo-29-1209-2011, 2011.

Laughman, B., Fritts, D. C., and Werne, J.: Numerical simulation of bore generation and morphology in thermal and Doppler ducts, Ann. Geophys., 27, 511–523, https://doi.org/10.5194/angeo-27-511-2009, 2009.

Li, Q., Xu, J., Yue, J., Liu, X., Yuan, W., Ning, B., Guan, S., and Younger, J. P.: Investigation of a mesospheric bore event over northern China, Ann. Geophys., 31, 409–418, https://doi.org/10.5194/angeo-31-409-2013, 2013.

Medeiros, A., Fechine, J., Buriti, R. A., Takahashi, H., Wrasse, C. M., and Gobbi, D.: Response of OH, O_2 and OI5577 airglow emissions to the mesospheric bore in the equatorial region of Brazil, Adv. Space Res., 35, 1971–1975, https://doi.org/10.1016/j.asr.2005.03.075, 2005.

Medeiros, A. F., Paulino, I., Taylor, M. J., Fechine, J., Takahashi, H., Buriti, R. A., Lima, L. M., and Wrasse, C. M.: Twin mesospheric bores observed over Brazilian equatorial region, Ann. Geophys., 34, 91–96, https://doi.org/10.5194/angeo-34-91-2016, 2016.

Mertens, C. J., Mlynczak, M. G., López-Puertas, M., Wintersteiner, P. P., Picard, R. H., Winick, J. R., Gordley, L. L., and Russell, J. M.: Retrieval of mesospheric and lower thermospheric kinetic temperature from measurements of CO_2 15 µm Earth Limb

Emission under non-LTE conditions, Geophys. Res. Lett., 28, 1391–1394, https://doi.org/10.1029/2000GL012189, 2001.

Mertens, C. J., Schmidlin, F. J., Goldberg, R. A., Remsberg, E. E., Pesnell, W. D., Russell, J. M., Mlynczak, M. G., López-Puertas, M., Wintersteiner, P. P., Picard, R. H., Winick, J. R., and Gordley, L. L.: SABER observations of mesospheric temperatures and comparisons with falling sphere measurements taken during the 2002 summer MaCWAVE campaign, Geophys. Res. Lett., 31, https://doi.org/10.1029/2003GL018605, l03105, 2004.

Mertens III, C. J., J. M. R., Mlynczak, M. G., She, C.-Y., Schmidlin, F. J., Goldberg, R. A., López-Puertas, M., Wintersteiner, P. P., Picard, R. H., Winick, J. R., and Xu, X.: Kinetic temperature and carbon dioxide from broadband infrared limb emission measurements taken from the TIMED/SABER instrument, Adv. Space Res., 43, 15–27, doi10.1016/j.asr.2008.04.017, 2009.

Nappo, C. J.: An Introduction to Atmospheric Waves, Academic Press, International Geophysics Series, Vol. 85, 279 pp., 2002.

Narayanan, V. L., Gurubaran, S., and Emperumal, K.: Nightglow imaging of different types of events, including a mesospheric bore observed on the night of February 15, 2007 from Tirunelveli (8.7° N), J. Atmos. Solar-Terr. Phys., 78/79, 70–83, https://doi.org/10.1016/j.jastp.2011.07.006, 2012.

Nielsen, K., Taylor, M. J., Stockwell, R., and Jarvis, M.: An unusual mesospheric bore event observed at hight latitudes over Antarctica, Geophys. Res. Lett., 33, L07803, https://doi.org/10.1029/2005GL025649, 2006.

Nielsen, K., Taylor, M. J., and Jarvis, M. J.: Climatology of short-period mesospheric gravity waves over Halley, Antarctica, (76° S, 27° W), J. Atmos. Solar-Terr. Phys., 71, 991–1000, https://doi.org/10.1016/j.jastp.2009.04.005, 2009.

Seyler, C. E.: Internal waves and undular bores in mesospheric inversion layers, J. Geophys. Res., 110, D09S05, https://doi.org/10.1029/2004JD004685, 2005.

Smith, S. M.: The identification of mesospheric frontal gravity-wave events at a mid-latitude site, Adv. Space Res., 54, 417–424, https://doi.org/10.1016/j.asr.2013.08.014, 2014.

Smith, S. M., Taylor, M. J., Swenson, G. R., She, C., Hocking, W., Baumgardner, J., and Mendillo, M. A.: Multidiagnostic investigation of the mesospheric bore phenomenon, J. Geophys. Res., 108, 13–18, https://doi.org/10.1029/2002JA009500, 2003.

Smith S. M., Stober G., Jacobi C., Chau J. L., Gerding M., Baumgardner J. L., Mendillo M., Lazzarin M., and Umbriaco G.: Characterization of a Double Mesospheric Bore Over Europe, J. Geophys. Res., 122, 9738–9750, https://doi.org/10.1002/2017JA024225, 2017.

Snively, J. B., Nielsen, K., Hickey, M. P., Heale, C. J., Taylor, M. J., and Moffat-Griffin, T.: Numerical and statistical evidence for long-range ducted gravity wave propagation over Halley, Antarctica, Geophys. Res. Lett., 40, 1–5, https://doi.org/10.1002/grl.50926, 2013.

Stockwell, R., Taylor, M. J., Nielsen, K., and Jarvis, M. A.: A novel joint space-wavenumber analysis of an unusual Antarctic gravity wave event, Geophys. Res. Lett., 33, L08805, https://doi.org/10.1029/2005GL025660, 2006.

Taylor, M. J., Turnbull, D. N., and Lowe, R. P.: Spectrometric and imaging measurements of a spectacular gravity wave event observed during the ALOHA-93 campaign, Geophys. Res. Lett., 20, 2849–2852, 1995.

Walterscheid, R. L., Hecht, J. H., Gelinas, L. J., Hickey, M. P., and Reid, I. M.: An intense traveling airglow front in the upper mesosphere–lower thermosphere with characteristics of a bore observed over Alice Springs, Australia, during a strong 2 day wave episode, J. Geophys. Res., 117, D22105, https://doi.org/10.1029/2012JD017847, 2012.

Wrasse, C. M., Takahashi, H., Medeiros, A. F., Lima, L. M., Taylor, M. J., Gobbi, D., and Fechine, J.: Determinação dos parâmetros de ondas de gravidade através da análise espectral de imagens de aeroluminescência, Braz. J. Geophys., 25, 257–266, 2007.